The American Journal of Pathology, Vol. 172, No. 4, April 2008

DOI: 10.2353/ajpath.2008.070605

Neurobiology

Blockade of Endothelinergic Receptors Prevents Development of Proliferative Vitreoretinopathy in Mice

María Iribarne,* Liliana Ogawa,* Vanesa Torbidoni,* Cristian M. Dodds,† Ricardo A. Dodds,*† and Angela M. Suburo*

From the Facultad de Ciencias Biomédicas, Universidad Austral, Pilar; and the Consultores Oftalmológicos,† Buenos Aires, Argentina*

Proliferative vitreoretinopathy (PVR) is characterized by severe glial remodeling. Glial activation and proliferation that occur in brain diseases are modulated by endothelin-1 (ET-1) and its receptor B (ETR-B). Because retinal astrocytes contain ET-1 and express ETR-B, we studied the changes of these molecules in an experimental mouse model of PVR and in human PVR. Both ET-1 and ETR-B immunoreactivities increased in mouse retina after induction of PVR with dispase. Epi- and subretinal outgrowths also displayed these immunoreactivities in both human and experimental PVR. Additionally, myofibroblasts and other membranous cell types showed both ET-1 and ETR-B immunoreactivities. In early stages of experimentally induced PVR, prepro-ET-1 and ETR-B mRNA levels increased in the retina. These mRNA levels also increased after retinal detachment (RD) produced by subretinal injection. Treatment of mice with tezosentan, an antagonist of endothelinergic receptors, reduced the histopathological hallmarks of dispase-induced PVR: retinal folding, epiretinal outgrowth, and gliosis. Our findings in human and in dispase-induced PVR support the involvement of endothelinergic pathways in retinal glial activation and the phenotypic transformations that underlie the growth of membranes in this pathology. Elucidating these pathways further will help to develop pharmacological treatments to prevent PVR. In addition, the presence of ET-1 and ETR-B in human fibrous membranes suggests that similar treatments could be helpful after PVR has been established. *(Am J Pathol 2008, 172:1030–1042; DOI: 10.2353/ajpath.2008.070605; DOI: 10.2353/ajpath.2008.070605)*

Despite progress in surgical procedures and adjuvant treatments, a significant incidence of proliferative vitreoretinopathy (PVR) can be expected even after successful surgery for primary or complicated retinal detachment (RD).[1,2] In PVR, cellular outgrowths or membranes develop on epi- and subretinal surfaces of the retina. Early development of these membranes associates to severe glial remodeling.[3,4] Müller glial cells show increased levels of the intermediate filament proteins, glial fibrillary acidic protein (GFAP) and vimentin.[5–7] Astrocytes also proliferate after experimental RD,[8] and their presence in human PVR membranes has been reported.[9–13] Retinal astrocytes normally express and accumulate endothelin-1 (ET-1),[14–16] a small peptide involved in glial activation[17] and development of fibrotic conditions.[18] Moreover, ET-1 increases in the vitreous humor and epiretinal membranes of PVR patients.[19] Therefore, astrocytes and ET-1 could play a central role in the pathogenesis of PVR.

Endothelins (ETs) are 21-amino acid peptides that derive from longer precursors.[20] The three ETs isoforms (ET-1, ET-2, and ET-3) have been found in the retina.[21,22] There are two endothelinergic receptors. ETR-A shows a particular affinity profile for each isoform (ET1 $\geq$ ET2 $\gg$ ET3), whereas ETR-B is equally responsive to all ETs.[20] ETR-B, however, is unique in its capacity to internalize bound ligand, reducing extracellular levels of ETs.[23]

We have previously demonstrated that both receptors appear in the mouse retina. ETR-A receptors are characteristically present in neuronal structures whereas ETR-B receptors mainly appear in astrocytes.[15,24] We have not been able to detect ET-1 or endothelinergic receptors in

Supported by the Universidad Austral, Roemmers Foundation, Consejo Nacional de Investigaciones Científicas y Técnicas, and grant PICT 2004/21399 from the Agencia Nacional de Promoción Científica y Tecnológica.

Accepted for publication December 20, 2007.

M.I. and V.T. are research fellows of the Consejo Nacional de Investigaciones Científicas y Técnicas, Argentina; A.M.S. is principal researcher at the same Institution; L.O. was a research fellow from Fundación Fiorini, Argentina.

Address reprint requests to Dr. Angela M. Suburo, Facultad de Ciencias Biomédicas, Universidad Austral, Pilar, Buenos Aires, B1629AHJ, Argentina. E-mail: amsuburo@cas.austral.edu.ar.

Table 1. Primary Antibodies Used in This Study

Antigen	Source	From
ET-1	Rabbit polyclonal	Peninsula Laboratories, Belmont, CA
ETR-B	Rabbit polyclonal	Alomone Labs, Jerusalem, Israel
pGFAP	Rabbit polyclonal	DAKO Labs, Carpinteria, CA
mGFAP	Mouse monoclonal	Bio Genex, San Ramon, CA
mGFAP-Cy-3 conjugate	Mouse monoclonal	Sigma-Aldrich, St. Louis, MO
Glutamine synthase	Rabbit polyclonal	Dr. A. Marmorstein, University of Arizona College of Medicine, Tucson, AZ
Cellular retinaldehyde binding protein (CRALBP)	Mouse monoclonal	Dr. J.C. Saari, University of Washington, Seattle, WA
Smooth muscle actin	Mouse monoclonal	Sigma-Aldrich
mSMA-Cy3 conjugate	Mouse monoclonal	Sigma-Aldrich
Opsin	Sheep polyclonal	Dr. D.S. Papermaster, University of Connecticut Health Center, Farmington, CT

Müller glial cells of normal BALB/c mice, although we have found ETR-B in these cells after light injury.[15,24] Other authors have reported the presence of ETR-B immunoreactivity in normal Müller cells of C57BL/6 mice and pigs.[22,25] ETR-B is also normally present in horizontal cells,[24] another participant in the retinal PVR response.[4]

To investigate involvement of endothelinergic pathways in PVR, we explored ET-1 and ETR-B immunoreactivities in experimentally induced murine PVR,[7] and human surgical specimens. Then we tested the effects of tezosentan, a blocker of endothelinergic receptors, on development of PVR-like lesions in mice.

Materials and Methods

PVR and RD Lesions in Mice

Experimental procedures were performed in male C57BL/6 mice (6 to 8 weeks old), following the Association for Research in Vision and Ophthalmology Statement for the Use of Animals. They were anesthetized with chloral hydrate (400 mg/kg, i.p.) and received one drop of 0.5% propacaraine (Alcon, Buenos Aires, Argentina) for local anesthesia. One drop of 5% phenylephrine and 1% tropicamide (Poen, Buenos Aires, Argentina) was applied for iris dilatation and eyes were covered with 0.25% carbomere (carboxypolymethylene) drops (Latlas; Atlas, Buenos Aires, Argentina). PVR-like lesions were induced as previously described,[7] using 3 μl of dispase (0.2 or 0.3 U/μl) intravitreal injections (Sigma-Aldrich, St. Louis MO). Fundus examinations were made in anesthetized animals with iris dilatation. Alternatively, hyaluronic acid (Hyasol; Bausch and Lomb, Buenos Aires, Argentina) was slowly injected through a 30-gauge needle, inserted below the limbus, until a detachment covering the dorsal quadrant could be observed. Procedures were performed at 8 p.m.[26] Animals were euthanatized 1 week after detachment. Membranes did not develop in this model.

Human PVR Membranes

Human specimens (n = 54, 40 epiretinal and 14 subretinal) were obtained from patients undergoing surgery for PVR. Use of human tissues adhered to World Medical Association Declaration of Helsinki and was approved by our Institutional Research Board.

Immunohistochemical Detection of Endothelinergic, Glial, and Smooth Muscle Markers

Human PVR membranes were flattened on a sterilized Millipore filter (Millipore, Billerica, MA) and immersed in a fixative mixture containing paraformaldehyde and picric acid in phosphate buffer.[27] Mice were deeply anesthetized (chloral hydrate, 800 mg/kg) and fixed by intracardiac perfusion with 4% paraformaldehyde in 0.1 mol/L phosphate buffer, pH 7.3. Specimens were cryoprotected[28] and frozen in N_2-cooled acetone. Sections (14 μm) were stained with Neutral Red or incubated with primary antibodies (Table 1).

Immunoenzymatic staining was done with biotinylated secondary antibodies and the avidin-biotin-horseradish peroxidase complex (Vector Elite; Vector Laboratories, Burlingame, CA). The latter was detected with diaminobenzidine and nickel enhancement.[29] Fluorescein isothiocyanate-, lissamine rhodamine-, or Cy5-conjugated anti-rabbit or anti-mouse IgGs (Jackson ImmunoResearch Laboratories, West Grove, PA) were used for immunofluorescence. The tyramide signal amplification system (Life Science Products, Boston, MA) was used for double immunostaining with two primary rabbit antibodies. Cy3-conjugated primary mouse monoclonals were used on mouse tissues to avoid false-positives caused by breaks of the retinal-blood barrier. Appropriate controls, omitting incubation with primary antibodies, were made for every immunostaining procedure.

Observations were made with a Nikon E-800 microscope (Nikon, Tokyo, Japan), fitted with filter blocks for fluorescein isothiocyanate, tetramethyl-rhodamine isothiocyanate, and Cy5. For confocal images we used a Radiance 2000 laser-scanning system (Bio-Rad, Hemel Hempstead, UK), applying the 488 line of the argon laser followed by the 543 line of a helium-neon laser, diode laser for excitation at 633 nm. Optical sections had 1 μm. Optic projections and merged images were produced

with the Confocal Assistant Software (Bio-Rad). To facilitate comparisons, endothelinergic molecules, smooth muscle actin (SMA), and GFAP were artificially colored in green, red, and blue, respectively.

Pharmacological Treatment

One hour after RD or dispase injection (0.3 U/μl), mice were randomly separated in two groups. Experimental mice received tezosentan (10 mg/kg, s.c., Actelion Pharmaceuticals, Zurich, Switzerland), a dual ET receptor antagonist,[30] and control mice received saline. Injections were repeated daily and mice were euthanatized after 7 days of treatment. Retinas were fixed for immunohistochemistry or freshly dissected for GFAP Western blots.

Reverse Transcriptase-Polymerase Chain Reaction (RT-PCR) Analysis

Retinal homogenates were prepared 3 days after RD or intravitreal dispase injection ($n = 4$ for each condition). Total RNA was extracted using RNeasy lipid tissue mini kit (Qiagen, Valencia, CA). RNA integrity was assessed by electrophoresis on a 1% agarose gel. Two μg of RNA was reverse-transcribed into cDNA with SuperScript II reverse transcriptase kit (Invitrogen, Carlsbad, CA) and oligo (dT) primers, following the manufacturer's recommendations. Each set of reactions always included a no-sample negative control.

Amplification of cDNA for preproET-1, ETR-B, and GAPDH as internal standard was performed with 35 PCR cycles (melting at 94°C for 30 seconds, annealing at 58°C for 30 seconds, extension at 72°C for 1 minute), using Platinum TaqDNA polymerase (Invitrogen). Trials were made to select the appropriate number of cycles so that amplification was in the exponential range and had not reached a plateau. The following specific primers were used: preproET-1 sense 5′-AGCTGGTGGAAGGAAGGAAACTACG-3′ and preproET-1 antisense 5′-GACAGTGCAGAAAGGTGAGGTAGACT-3′; ETR-B sense 5′-GGCTAGTGTGTTTTCAGAGGCTTG-3′ and ETR-B antisense 5′-CAGAACCACAGAGACCACCCAAAT-3′; GAPDH sense 5′-ACCACAGTCCATGCCATCAC-3′ and GAPDH antisense 5′-TCCACCACCCTGTTGCTGTA-3′. PCR products were analyzed by electrophoresis on a 1% agarose gel and the expected sizes of amplicons were 728 bp for preproET-1, 822 bp for ETR-B, and 452 bp for GAPDH.

Quantitative Evaluation of Retinal Folding and Membrane Growth

Eyes were sectioned serially. Every third section (~24 to 26 sections per eye) was incubated with the polyclonal GFAP antiserum and developed with the immunoenzymatic procedure. To compare the severity of dispase-induced lesions, each section was examined by a blinded observer who determined the presence or absence of retinal folds, epi- or subretinal membranes. We applied the following score: presence of folds, 1; presence of epiretinal membrane, 1 (or 2 for membranes larger than half retina); presence of subretinal membrane, 1. The total score for each eye divided by the number of sections gave an average score reflecting the presence and extension of lesions in each eye. Comparisons were made with two-way analysis of variance with Bonferroni posttests (GraphPad Prism version 4.00 for Windows; GraphPad Software, San Diego, CA).

GFAP Western Blot Analysis

Retinas (two per sample) were homogenized in an extraction buffer containing 10 mmol/L Tris-HCl with 2 mmol/L ethylenediaminetetraacetic acid, 150 mmol/L NaCl, 1% Triton X-100, and protease inhibitor cocktail (Sigma-Aldrich). Extracts (30 μg of protein per lane) were separated by sodium dodecyl sulfate-polyacrylamide gel electrophoresis and transferred (100 v, 90 minutes) onto a nitrocellulose filter using standard techniques. Equal sample loading for electrophoresis was confirmed by the Bradford protein assay (Sigma-Aldrich) and equal transfer to the membrane was confirmed by Ponceau S staining. Immunoblotting was performed with mGFAP antibody. The membrane was further incubated with biotinylated anti-mouse IgG and extravidin-alkaline phosphatase. Colorimetric detection of alkaline phosphatase was made with 5-bromo-4-chloro-3-indolyl-phosphate and nitro blue tetrazolium (Sigma-Aldrich). Optical density was estimated using Scion Image β 4.02 Win software (Scion Corp., Frederick, MD). Analysis of variance and *t*-test for paired samples were used for statistical comparisons (GraphPad Prism version 4.00 for Windows).

Results

Dispase-Induced PVR

We have previously shown[7] that mice receiving intravitreal dispase (0.2 U/μl) gradually develop a PVR-like condition. Retinal folds appear during the first and second weeks after injection whereas epiretinal membranes appear after the second week in ~60 percent of the injected eyes. Therefore, we evaluated distribution of ET-1 and GFAP immunoreactivity 7, 14, or 21 days after intravitreal injection ($n = 10$ for each stage). Control C57BL/6 mice showed the same pattern of ET-1, ETR-B, and GFAP immunoreactivities previously described in BALB/c mice.[15] Astrocytes displayed strong ET-1 and GFAP immunoreactivity, whereas normal Müller cells lacked ET-1 and GFAP immunoreactivity (Figure 1, A and B).

Retinal Folding and Outgrowths

After dispase injection, a thick layer of ET-1- and GFAP-immunoreactive processes appeared along the vitreal surface. Similar processes extended into deeper layers of the retina, usually following an irregular course (Figure 1, C and D). They could perhaps correspond to in-growing astrocyte branches because they were not labeled by typical Müller cell markers, such as CRALBP

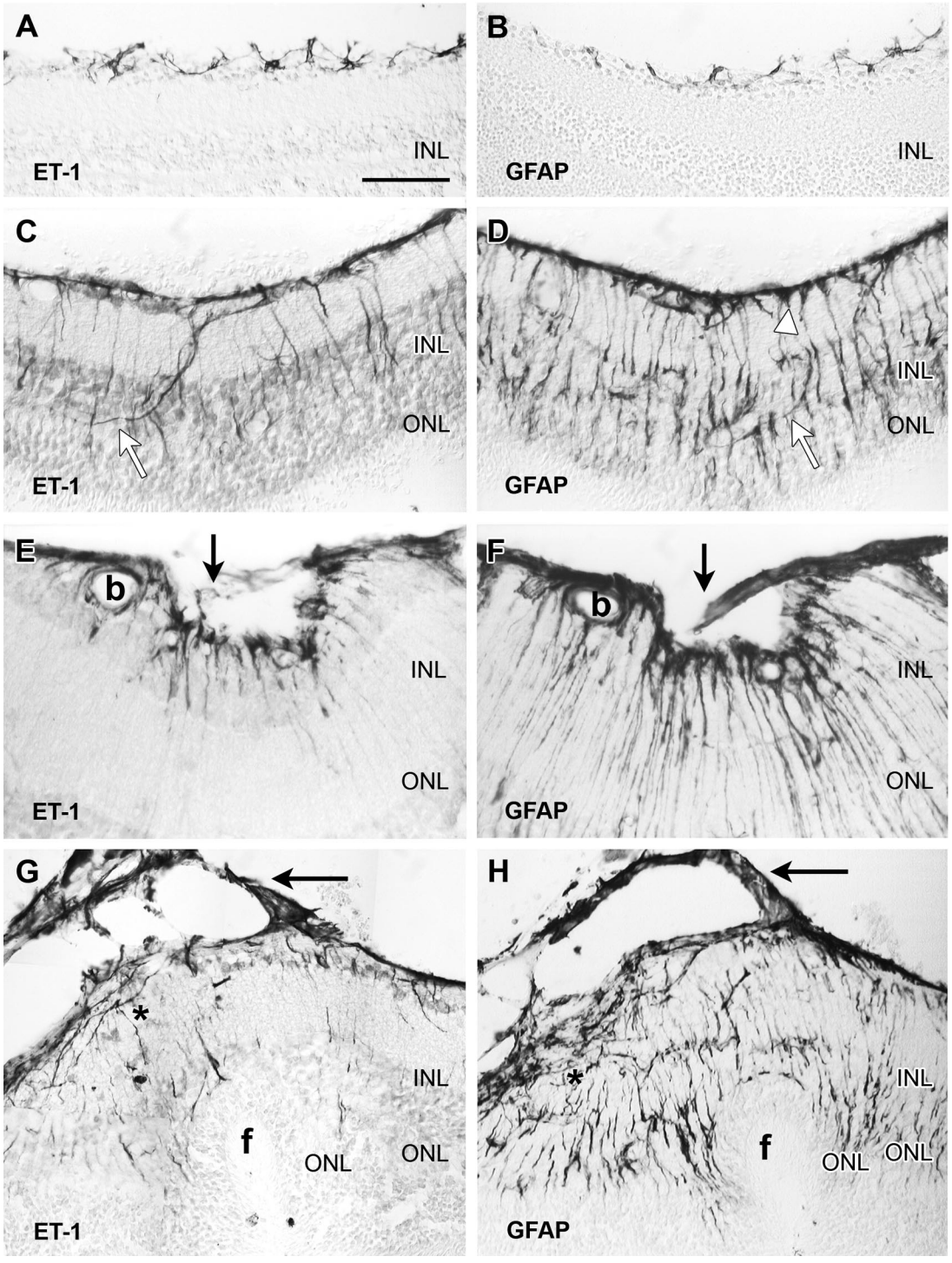

Figure 1. Consecutive sections of mouse retina immunoenzymatically stained with antibodies against ET-1 (**left**) and GFAP (**right**). The retinal vitreal surface is always shown at the **top** of the micrographs. **A** and **B:** In the normal retina, ET-1 immunoreactivity was only found in astrocytes sparsely distributed along the vitreal surface. GFAP immunostaining labeled similar cell bodies and processes. **C** and **D:** These and following images correspond to 0.2 U/μl dispase-injected eyes. One week after injection, the vitreal surface was completely covered by ET-1-immunoreactive astrocyte cell bodies and processes. Irregular ET-1-immunoreactive processes, following a nonradial course, extended into outer layers of the retina (**white arrows**). GFAP immunolabeled structures along the vitreal surface included astrocytes and Müller endfeet (**white arrowhead**). Notice the large number of GFAP-immunoreactive processes extending to the outer retinal layers. Most of them followed the typical radial course of Müller cells, but a few resembled endothelinergic processes (**white arrows**). **E** and **F:** Illustration of an inner retinal fold bridged by a small outgrowth (**arrows**), appearing a week after dispase injection. Strong ET-1 and GFAP immunoreactivities appeared along the vitreal border, within the outgrowth and in retinal processes. GFAP revealed a larger number of processes than ET-1. Immunostained glial cells also surrounded a blood vessel (b). **G** and **H:** Retina sections (2 weeks after dispase) showing an outer fold (f). A thin cellular membrane (**arrows**) attached to the vitreal surface exhibited strong ET-1 and GFAP immunostaining. Elongate ET-1- and GFAP-immunoreactive cells were accumulated along the retinal vitreal surface (**asterisk**). Immunoreactive processes extended across the retina: few endothelinergic processes reached the invaginated ONL, whereas numerous GFAP-immunoreactive processes appeared close to the subretinal folded surface. Scale bar: 50 μm (**A–E**, **G**, **H**); 25 μm (**F**).

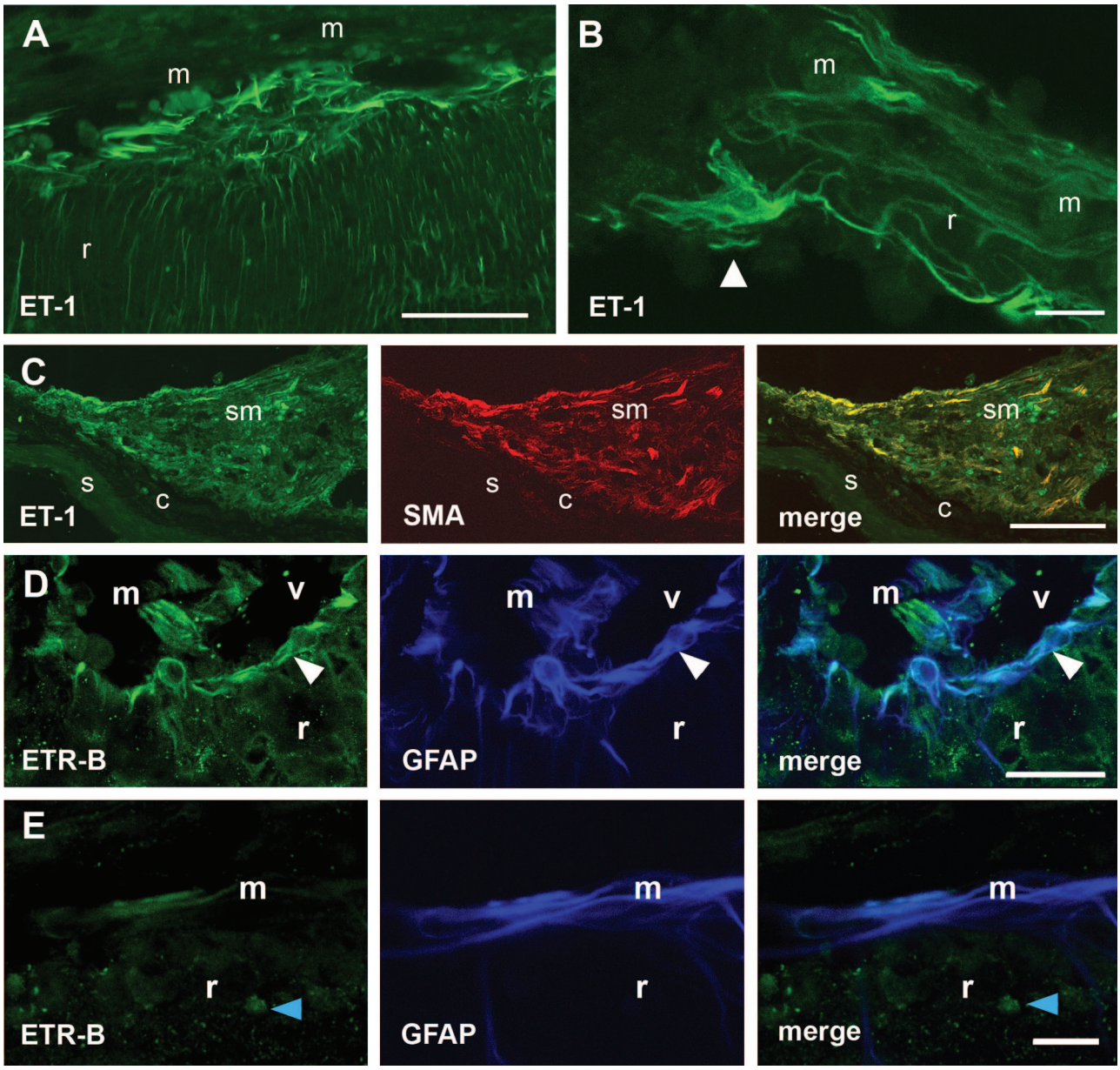

Figure 2. ET-1 and ETR-B immunofluorescence in epi- and subretinal outgrowths appearing 2 weeks after 0.2 U/μl dispase intravitreal injection. **A:** Strong ET-1 immunofluorescence appeared in a region of disrupted ILM, where the vitreal surface was attached to an epiretinal membrane (m). Notice the thick endothelinergic processes parallel to the surface and the large number of thinner processes within the retina. **B:** In a membrane attached to the vitreal surface, an ET-1-immunoreactive cell could be identified as an astrocyte by its shape and planar distribution of cell processes. Numerous endothelinergic processes appeared within the membrane. r, retina. **C:** Confocal images of a subretinal membrane (sm) attached to the choroid (c). Numerous cells exhibiting ET-1 (green) and SMA (red) immunofluorescence can be observed. Merging demonstrates co-localization of both markers in elongate cells probably corresponding to myofibroblasts. s, sclera. **D:** Confocal images through the inner retina (r) showed ETR-B-immunoreactive cell bodies and processes placed along the vitreal surface (**white arrowhead**). GFAP antiserum labeled the same structures. Some radial processes were labeled by only one of these markers. An epiretinal membrane (m) appearing within the vitreal (v) space showed almost complete segregation of ETR-B and GFAP immunofluorescence. **E:** Confocal images through an epiretinal membrane attached to the retinal surface showed a few ETR-B-immunoreactive cells. GFAP labeled a larger group of elongate cells. The merged image demonstrated that these ETR-B-immunoreactive cells also had GFAP immunoreactivity, whereas most GFAP-immunoreactive cells lacked ETR-B immunofluorescence. The **blue arrowhead** points to an ETR-B-immunoreactive cell nucleus. Scale bars: 50 μm (**A**, **B**); 100 μm (**C**); 25 μm (**D**, **E**).

and GS antibodies (not shown). By contrast, most GFAP-immunoreactive processes followed the typical radial course of Müller glia and lacked ET-1 immunoreactivity.

Retinal folds appeared before RD or membrane development. Inner folds showed strong ET-1 and GFAP immunostaining of vitreal glial structures (Figure 1, E and F). Outer folds presented as invaginations of outer retinal layers with a small detachment restricted to the base of the folding (Figure 1, G and H). Vitreal outgrowths appeared 1 or more weeks after dispase injection. They usually attached to disrupted regions of the inner limiting membrane (ILM) and included ET-1- and GFAP-immunoreactive cells (Figure 1, E–H).

Epi- and subretinal fibrous membranes were usually observed at later stages. ET-1-immunofluorescent structures occupied the boundary between retina and epiretinal membranes, and also appeared within the retina (Figure

2, A and B). Subretinal outgrowths also contained ET-1-immunoreactive cells. In fibrous membranes, SMA-immunoreactive cells often showed ET-1 immunostaining (Figure 2C). GFAP-immunoreactive cells were also present, but they seldom displayed ET-1 labeling (not shown).

ETR-B Immunoreactivity

In control retinas, weak ETR-B immunoreactivity was only found in astrocytes (see below). After dispase injection, stronger ETR-B immunoreactivity appeared in astrocytes lying along folded vitreal surfaces (Figure 2D). Most retinal structures also showed GFAP immunoreactivity, suggesting a relationship with astrocytes or Müller cells. Epiretinal processes (Figure 2, D and E) also showed ETR-B immunoreactivity, but only a fraction of them also displayed GFAP immunoreactivity. Widespread immunostaining of cell nuclei[15,31,32] hindered identification of cells with selective cytoplasmic localization of ETR-B immunofluorescence. Although mouse fibrous membranes contained ETR-B-immunofluorescent cells, we could not demonstrate its co-localization with SMA immunoreactivity.

Human Specimens

Retina

A few surgical specimens ($n = 4$) contained small patches of retinal tissue. These fragments always showed histoarchitectural disorganization, but Nomarski optics or staining with Neutral Red allowed recognition of retinal layering. Opsin immunoreactivity identified photoreceptor outer segments (not shown). Some fragments showed a thin layer of ET-1-immunoreactive cells along the vitreous surface, whereas other fragments displayed this immunoreactivity in more extensive areas (Figures 3A and 4A). GFAP immunoreactivity occupied the same regions and often co-localized with ET-1 immunoreactivity. The regular GFAP-immunoreactive pattern of the ILM disappeared at sites of membranous outgrowth attachment to the retinal vitreal surface. Membranous outgrowths showed both ET-1 and GFAP immunoreactivity (Figures 3 and 4A).

Membranes

Fibrous and nonfibrous regions differed in amount of extracellular matrix. Nonfibrous regions of epi- and subretinal membranes contained many ET-1- and GFAP-immunoreactive cells but few SMA-immunolabeled cells. Fibrous regions contained numerous ET-1- and SMA-immunoreactive cells. Co-localization proved that these cells were endothelinergic myofibroblasts (Figure 4B). By contrast, we could not detect co-localization of ET-1 and GFAP immunoreactivities in fibrous membranes. Neither did we find examples of co-localization of ET-1 and CRALBP or GS immunofluorescence.

Human PVR membranes also contained many ETR-B-immunoreactive cells. They often showed an elongate phenotype arranged in regular layers (Figure 4, C–G). SMA-immunoreactive myofibroblasts with and without ETR-B immunoreactivity were present in the same membrane (Figure 4, E–G). By contrast, human fibrous membranes seldom contained cells displaying both ETR-B and GFAP immunofluorescence (Figure 4H). No significant differences were detected between epi- and subretinal membranes.

Blockade of ET Receptors and Development of PVR-Like Lesions

Testing showed that intravitreal injection of 0.3 U/μl dispase in mice 8 weeks old (or younger) induced membrane growth in every eye after just 1 week. Therefore, we used this procedure to evaluate the effects of tezosentan. In animals receiving saline, all specimens had large RDs. Their retinas showed inner and outer retinal folds, and had

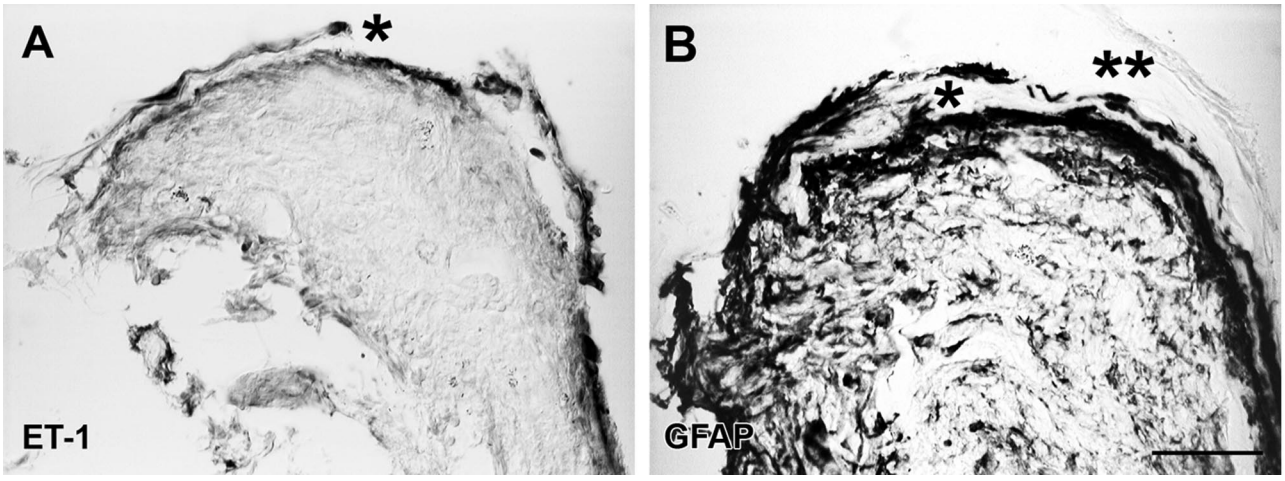

Figure 3. Sections through a retinal fragment embedded in a human PVR specimen labeled with the immunoenzymatic method and examined under Nomarski optics. **A:** ET-1 immunoreactivity appeared along the vitreal surface of a highly disorganized retinal fragment. An epiretinal outgrowth (**asterisk**) separated from the inner retinal surface also showed strong ET-1 immunoreactivity. **B:** A section through the same fragment (not consecutive) showed extensive GFAP immunoreactivity in most retinal layers. GFAP-immunoreactive cells were present in an outgrowth (**asterisk**) apparently emerging from the retinal surface. A neighboring outgrowth (**asterisks**) had no immunoreactivity. Scale bar: 50 μm.

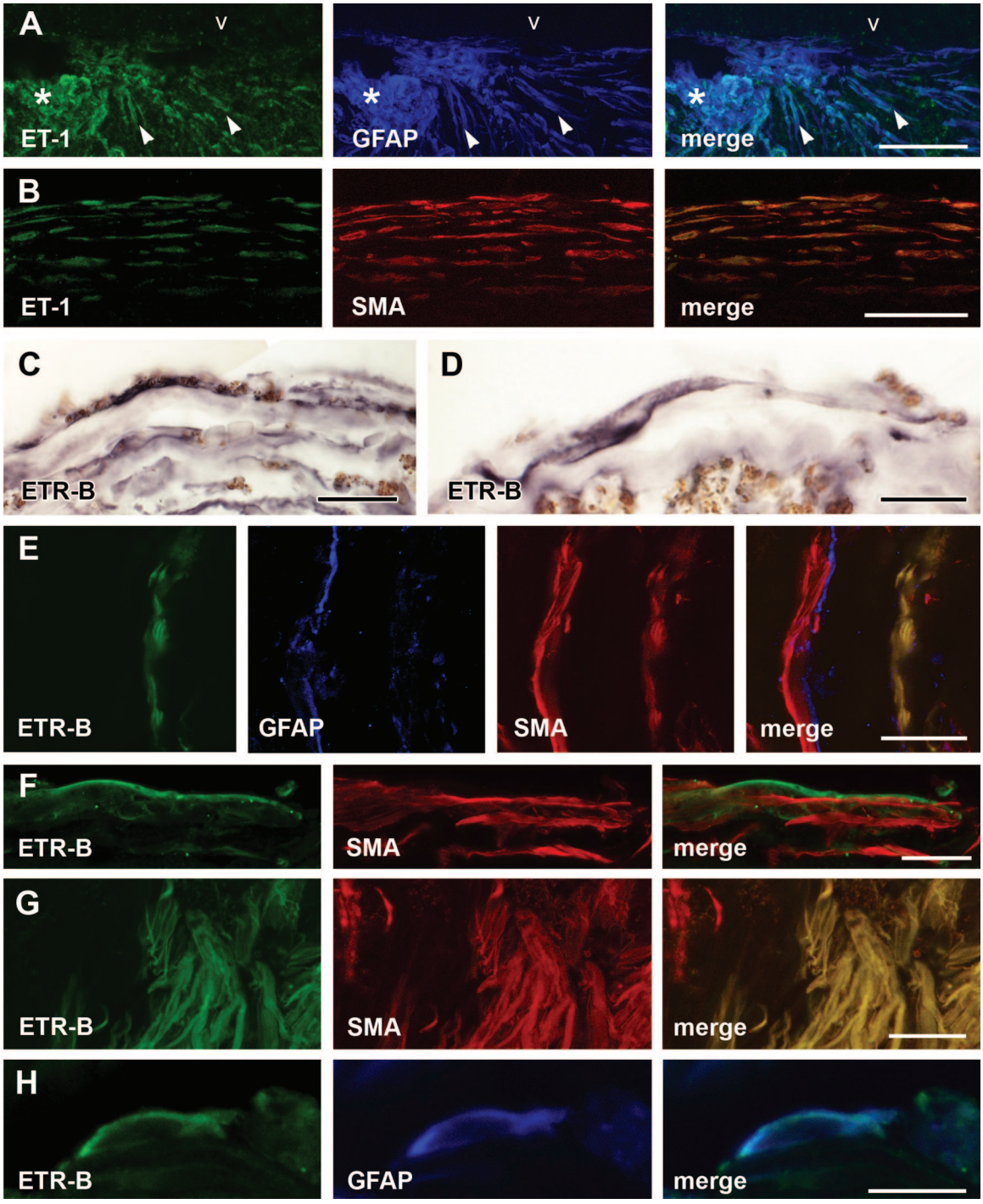

Figure 4. ET-1- and ETR-B-immunoreactive cells in human specimens. **A:** Confocal images through a retinal fragment embedded in a human epiretinal membrane showed an epiretinal outgrowth (**asterisk**) displaying strong ET-1 immunoreactivity. ET-1-immunoreactive cells followed radial pathways across the retina (**arrowheads**) or coursed along its vitreal surface (v). GFAP immunofluorescence essentially labeled the same structures. However, some GFAP-immunoreactive cells lacked ET-1 immunofluorescence. **B:** Confocal images of a fibrous human epiretinal membrane showing elongate cells arrayed in parallel layers. These cells displayed both ET-1 and SMA immunofluorescence as demonstrated in the merged image. **C:** The immunoenzymatic procedure demonstrated elongate ETR-B-labeled arrayed in parallel layers. **D:** This view of a fibrous membrane showed a long ETR-B-immunoreactive cell parallel to the surface of the membrane. The membrane contained abundant pigmented granules. **E:** Confocal images of a fibrous membrane showed a layer of ETR-B cells. A different cell layer displayed GFAP immunofluorescence. Both layers had SMA immunoreactivity. ETR-B co-localized with SMA in cells of the first layer (**right**). In the second layer, GFAP immunofluorescence was segregated from SMA. **F:** Elongate cells displayed ETR-B immunofluorescence. SMA immunoreactivity appeared in cells of similar shape. However, no co-localization could be detected in these cells. **G:** Another membrane showed a large cluster of ETR-B-immunoreactive cells. The same cells also displayed SMA immunofluorescence. However, a neighboring group of SMA-immunoreactive cells (**left**) was not labeled by ETR-B. **H:** An isolated cell displaying ETR-B immunofluorescence also showed GFAP immunoreactivity. Merge demonstrates co-localization. Scale bars: 25 μm (**A**, **C**, **E–G**); 50 μm (**B**); 15 μm (**D**, **H**).

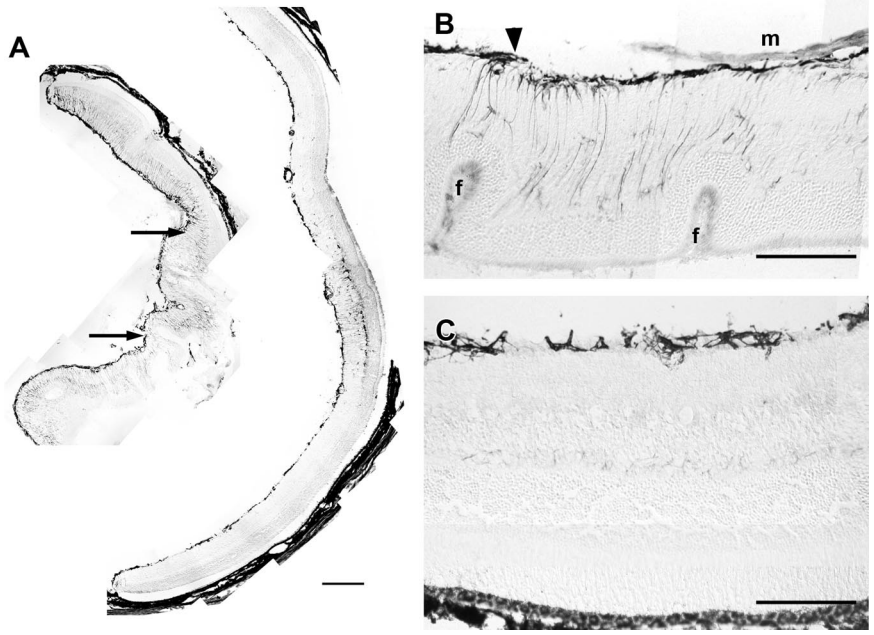

Figure 5. A: These low-magnification montages of GFAP-immunostained retinal cryosections show the effect of tezosentan treatment on retinal lesions appearing 1 week after 0.3 U/μl dispase injection. The retina from an untreated mouse (**left**) displayed severe folding. **Arrows** point to epiretinal membranes. Large areas of the inner retina displayed strong GFAP immunoreactivity. The retina from a mouse receiving tezosentan (**right**) had no folds. The vitreal surface showed increased GFAP immunoreactivity. GFAP immunostaining of the inner retina was only found at a small region of the retina. **B:** Outer retinal folds (f) and an epiretinal membrane were present in this untreated retina. GFAP-immunoreactive structures form a thick layer along the vitreal surface and extend toward the outer retina. The **arrowhead** points to a GFAP-immunoreactive vitreal outgrowth. **C:** This retina from a treated animal appeared well attached to the RPE and showed good preservation of retinal layering. GFAP-immunoreactive structures were restricted to the vitreal surface. Scale bars: 200 μm (**A**); 60 μm (**B**, **C**).

epi- and subretinal membranes. By contrast, retinal folding and membrane growth were minimal in animals receiving tezosentan (Figure 5), although some of these retinas exhibited large detachments. Quantitative analysis of these features (Table 2) indicated that tezosentan treatment significantly reduced the scores for folds ($P < 0.01$) and epiretinal membranes ($P < 0.01$). Decrease of subretinal membranes was not statistically significant. Remarkably, subretinal membranes did not contain ETB-R immunoreactivity whereas ETB-R-immunoreactive cells were found within epiretinal membranes and along the boundary between these membranes and the retina (Figure 6).

Comparison of GFAP immunostaining in tezosentan- and saline-treated animals suggested a decrease of retinal gliosis. Western blots showed a trend toward lower GFAP levels in tezosentan-treated mice. However, differences were not statistically significant (Figure 7), probably because high GFAP immunostaining was still found in regions of detachment and subretinal membranes. Because downregulation of GFAP could be one of the factors decreasing retinal folding, we measured GFAP protein in retinas detached by subretinal injections of hyaluronic acid. These retinas expressed higher GFAP levels than those subjected to dispase injection. Mice receiving tezosentan after RD had ~50% of the GFAP levels found in saline-treated mice (Figure 7).

Table 2. PVR Lesions after Treatment with Tezosentan

Lesions	Saline	Tezosentan
Retinal folds	0.73 ± 0.13	0.14 ± 0.07
Epiretinal membranes	0.78 ± 0.22	0.10 ± 0.07
Subretinal membranes	0.62 ± 0.13	0.41 ± 0.14

Dispase-induced lesions in eyes from saline- or tezosentan-treated animals scored in GFAP-immunostained sections as described in the Materials and Methods. Values represent the average for seven eyes (from five animals) ± SEM. Two-way analysis of variance indicated that the effect of treatment was highly significant ($P = 0.0001$). Bonferroni post-tests indicated that scores for retinal folds and epiretinal membranes were statistically significant, $P < 0.01$ and $P < 0.05$, respectively.

Early Changes of ET-1 and ETR-B after Dispase Intravitreal Injection or RD

Because endothelinergic activation and glial transformation should precede development of epi- or subretinal outgrowths, we also evaluated early stages of murine PVR. RT-PCR showed that prepro-ET-1 and ETR-B mRNAs highly increased 3 days after 0.3 U/μl dispase injection (Figure 8), before membranous outgrowths

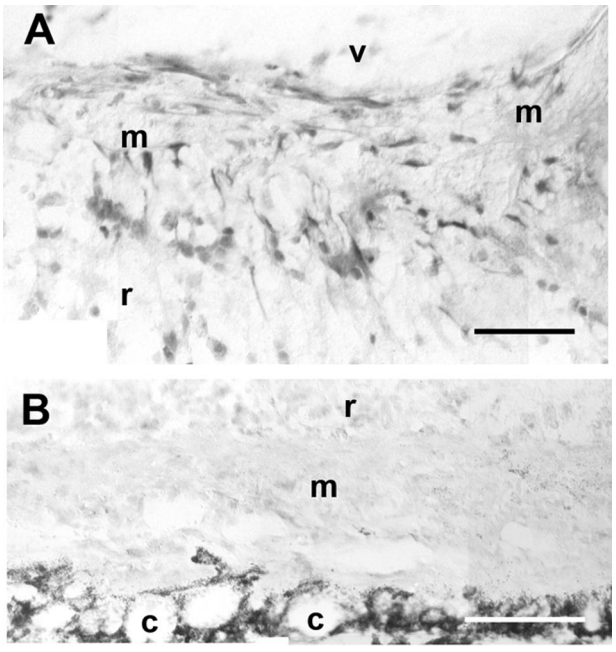

Figure 6. ETR-B immunoreactivity in mouse epi- and subretinal membranes developing 1 week after 0.3 U/μl dispase injection. **A:** This epiretinal membrane (m) was attached to the retinal surface and exhibited numerous ETR-B-immunoreactive cells. v, vitreal space; r, retina. **B:** A subretinal membrane (m), lodged between the retina (r) and the choroid (c), lacked ETR-B immunostaining. Scale bars: 50 μm (**A**); 100 μm (**B**).

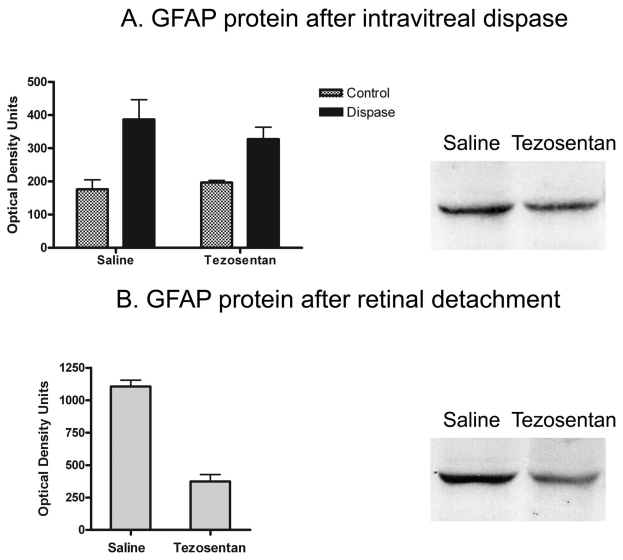

Figure 7. A: Differences of GFAP protein levels in control and dispase-injected eyes, receiving saline or tezosentan (each group, $n = 4$), were evaluated with two-way analysis of variance. Tezosentan did not increase GFAP protein in control mice. Dispase injection (0.3 U/μl) produced a significant increase of GFAP protein ($P < 0.01$). This increase was not affected by tezosentan treatment. Bands corresponding to a pair of saline- and tezosentan-treated dispase-injected eyes showed similar immunostaining. **B:** A large increase of GFAP protein followed RD. Tezosentan treatment significantly reduced these levels. Paired *t*-test ($n = 8$ pairs, $P < 0.0004$). The bands corresponding to a pair of saline- and tezosentan-treated RD samples illustrate this large reduction.

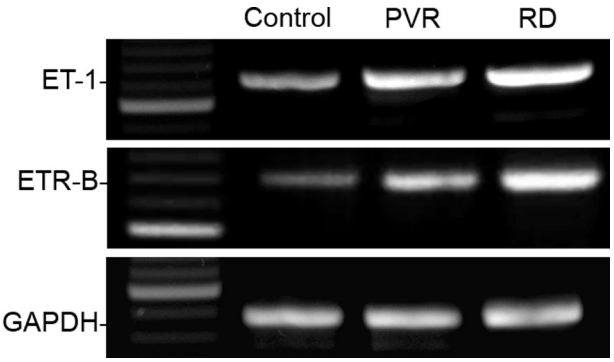

Figure 8. Effect of experimental PVR and RD on amplification of retinal prepro-ET-1, ETR-B, and GADPDH mRNA sequences. Extracts were prepared 3 days after each procedure. Intensity of the prepro-ET-1 and ETR-B amplification products increased after experimental PVR and RD. Both bands were always stronger after RD than after PVR. Intensity of the GAPDH amplification product did not change significantly.

could be detected. An increase was also found after experimental RD, a condition followed by spontaneous reattachment without membrane development.

Immunohistochemistry ($n = 4$ for each group) showed the presence of retinal folds 3 days after dispase injection (0.3 U/μl). Astrocytes showed strong ET-1 and ETR-B immunolabeling. They had thick processes that often extended into the vitreal cavity, suggesting early disruption of the ILM (Figure 9, A and B, E and F). No folds were observed after RD. Astrocytes displaying strong ET-1 immunolabeling were more often found in control retinas (Figure 9, C and D). ETR-B immunoreactivity strikingly increased in astrocytes and, in some retinal regions, also in Müller cells (Figure 8, G and H). Evidence of ILM disruption was not found in RD specimens.

Discussion

Our findings in human and experimental PVR showed the presence of cells expressing ET-1 and ETR-B in these lesions. An involvement of endothelinergic pathways in development of PVR is supported by prevention of retinal folding and growth of epiretinal membranes in mice treated with tezosentan, a mixed antagonist of endothelinergic receptors.

Endothelinergic Cells, Endothelinergic Receptors, and Development of PVR

Among normal retinal cells of BALB/c mice, astrocytes present the highest ET-1 immunoreactivity.[15] These observations have now been confirmed in C57BL/6 mice. ET-1 immunoreactivity in astrocytes and their processes increased after PVR-like lesions induced by 0.2 and 0.3 U/μl dispase intravitreal injection, and after RD produced by hyaluronic acid subretinal injection. In PVR-like lesions, astrocytes also displayed an abnormally high number of cell processes. These processes extended into the vitreal cavity when disruption of the ILM was present. This is not surprising, because astrocytes migrating through focal interruptions in the ILM were identified in early descriptions of massive periretinal proliferation.[33]

Three days after intravitreal dispase injection, astrocytes showed a large increase in ET-1 and ETR-B immunoreactivity that was accompanied by prepro-ET-1 and ETR-B mRNA up-regulation in the retina. The simultaneous increase of ET-1 and ETR-B suggests that astrocytes would be activated by an autocrine mechanism. Extension of astrocytic processes into the vitreal cavity would be the first step in epiretinal membrane development. Prevention of retinal folding and epiretinal membrane growth by the endothelinergic antagonist tezosentan would then be explained by blockade of these autocrine mechanisms. Subretinal membrane growth would still be possible because they lacked ETR-B, at least in the dispase model. Further studies with selective antagonists are required to understand the role of each endothelinergic receptor in PVR. Although we have not observed glial ETR-A in the retina,[15,24] co-existence of both receptors has been reported in brain astrocytes *in vitro*.[34] In addition, some endothelinergic effects on astrocytes and fibroblasts require the simultaneous participation of both receptors.[35,36]

A Model to Explain Endothelinergic Involvement in Retinal Folding and Membrane Growth

ET-1-immunoreactive astrocytes appear in mechanically deformed regions of the brain. In addition, stretching astrocyte cultures causes an increase in ET-1 production and secretion into the culture media.[37,38] Most brain astrocytes do not express ET-1 under normal conditions. By contrast, retinal astrocytes always show strong ET-1 immunoreactivity, even in the absence of injury. Because

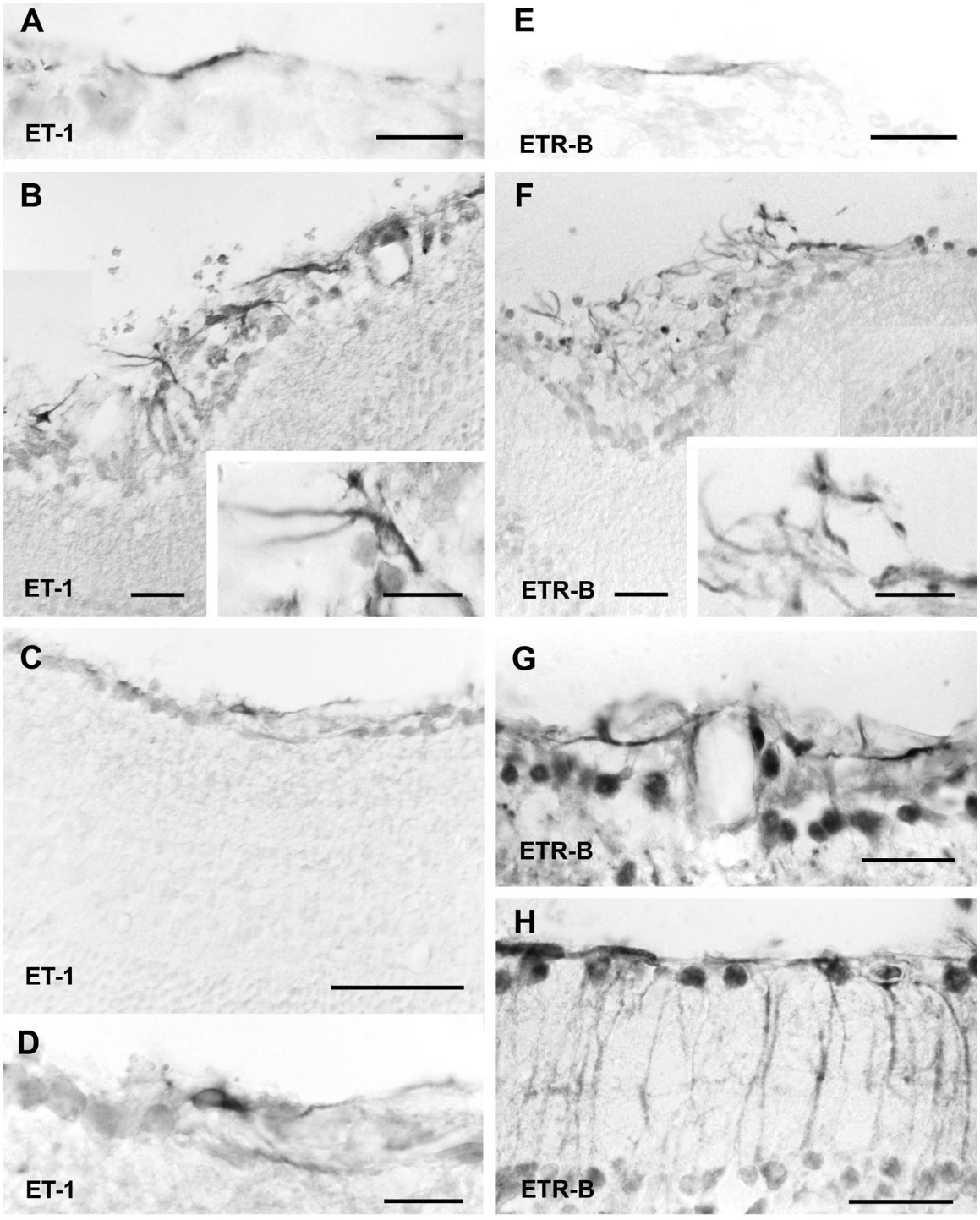

Figure 9. Immunoreactivity of ET-1 (**left**) and ETR-B (**right**) was demonstrated by the immunoenzymatic procedure 3 days after RD or dispase injection (0.3 U/μl). Images were acquired with Nomarski optics. **A:** This high-power view, corresponding to a normal retina, showed that isolated astrocytic processes were present. **B:** A retinal fold induced by dispase injection, showed numerous ET-1-immunostained astrocytes. The ILM had disappeared and astrocyte processes invaded the vitreal space. The **inset** illustrates the large size of these astrocytes. **C** and **D:** Low- and high-power views of ET-1 immunoreactivity after RD. ET-1 was moderately increased and could only be detected in astrocytes. **E:** This high-power view showed weak ETR-B immunoreactivity in astrocytic processes of control retinas. **F:** After dispase injection, numerous ETR-B-immunoreactive astrocytes appeared along the vitreal surface of the retina. In regions of ILM disruption, numerous astrocytic processes extended into the vitreal space. **G** and **H:** These images correspond to detached retinas. Notice the preservation of the ILM in both examples. **G** shows perivascular astrocytes displaying strong ETR-B immunoreactivity. **H** shows a retinal region displaying ETR-B immunoreactivity in astrocytes and Müller cells. Cell nuclei were also strongly immunostained in these preparations. Scale bars: 15 μm [**A**, **B** (inset), **D**, **E**, **F** (**inset**)]; 25 μm (**B**, **F–H**); 50 μm (**C**).

retinal astrocytes lie at the retino-vitreal boundary, their high ET-1 expression might reflect stretching forces acting on that concave surface. Any disruption of the ILM, as that occurring after dispase injection, would stretch astrocytes and increase ET-1 synthesis. This would potentiate the production and secretion of more ET-1, as has been described in other systems.[39] Disruption of the ILM would not necessarily depend on endothelinergic up-regulation. However, inhibition of endothelinergic pathways could prevent vitreal outgrowth, even in the presence of ILM injury.

ET-1 controls astrocytic proliferation,[40] probably through ETR-B stimulation.[34,41,42] Besides, ETR-B receptors could perhaps mediate a similar mitogenic effect of ET-1 on Müller cells. Thus, the progressive gliosis of PVR could be relentlessly driven by the continuous secretion of ET-1 initiated in astrocytes. Blockade of endothelinergic receptors by tezosentan would inhibit that autocrine mechanism as well as the mitogenic and hypertrophic effects of ET-1. Decrease of GFAP expression would also help to break this pathogenic loop, since it has been demonstrated that lack of GFAP limits glial hypertrophy and up-regulation of ETR-B receptors.[43,44]

Folding of the retina is an early event in experimental PVR,[7] implying that changes in retinal cell shape occur before membranes grow. Tezosentan treatment significantly decreased retinal inner and outer folding, even in the presence of a large RD. Cytoskeletal regulation is another well known effect of ET-1, and astrocytes exposed to this peptide up-regulate actin- and microtubule-associated protein.[45]

Endothelins could also engage in the phenotypical changes involved in the differentiation of fibroblast- and myofibroblast-like cells forming the core of PVR membranes. ET-1 is required to induce the epithelial-mesenchymal transition of cancer cells[46] and promotes fibroblast synthesis of collagen types I and III in normal fibroblasts.[47] ET-1 also induces the fibrogenic phenotypes characteristic of lesional systemic sclerosis fibroblasts and pulmonary fibrosis through mechanisms dependent on both ETR-A and ETR-B receptors.[36,47] In addition, ET-1 is involved in myofibroblast differentiation, contraction and migration.[48,49]

Epi- and Subretinal Membranes

Epi- and subretinal membranes contained ET-1-immunoreactive cells. Some ET-1-immunoreactive cells also showed GFAP immunoreactivity. These cells were usually placed in early vitreal outgrowths or boundaries between retina and epiretinal membrane. By contrast, in fibrous regions, ET-1 immunoreactivity often co-localized with SMA immunoreactivity. Transformation of astrocytes in myofibroblasts is a likely possibility. SMA has been previously detected in astrocytes,[50] whereas loss of GFAP immunoreactivity has been reported after myofibroblast transformation of porcine Müller cells *in vitro*.[51] Myofibroblasts could also arise from other cells involved in PVR development, such as macrophages and retinal pigment epithelial cells[52,53] that also can express ET-1.[54]

PVR membranes also included ETR-B-immunoreactive cells. In human membranes, a fraction of these cells corresponded to a subpopulation of myofibroblasts. In mice, co-localization of ETR-B with GFAP or SMA was seldom found. Thus, more studies are needed to identify the phenotypical identity of membranous ETR-B-immunoreactive cells. This could be of therapeutical importance, because endothelinergic blockade might also be effective in the prevention of fibrosis and tractional RD.

The importance of ETR-B receptors for membrane growth is also reflected by persistence of mouse subretinal membranes, which had no detectable ETR-B immunoreactivity, after treatment with tezosentan. Differences between epi- and subretinal membrane are well known.[3] In the mouse dispase model, only subretinal membranes contain RPE cells.[7] However, human subretinal membranes had ETR-B-immunoreactive cells, suggesting that cells within these membranes could differentiate into this phenotype. Alternatively, the RPE could release chemoattractants for astrocytes.[55,56]

Conclusions

Our findings support the involvement of ET receptors in development of PVR typical lesions, namely, glial activation, retinal folding, and membrane growth. Further studies are needed to understand the importance of different retinal autocrine and paracrine loops, as well as the contribution of each ET isoform to PVR pathogenesis. Answering these questions will help to develop pharmacological treatments preventing PVR development, particularly in high-risk cases. In addition, the presence of ET-1 and ETR-B in human fibrous membranes suggests that similar treatments could be helpful after PVR has been established.

Acknowledgments

We thank Guillermo Gastón, Germán Ruffolo, Silvina Ruffolo, and Soledad Arregui for their skillful technical assistance.

References

1. Charteris DG, Sethi CS, Lewis GP, Fisher SK: Proliferative vitreoretinopathy—developments in adjunctive treatment and retinal pathology. Eye 2002, 16:369–374
2. Scott IU, Flynn HW Jr, Murray TG, Feuer WJ: Outcomes of surgery for retinal detachment associated with proliferative vitreoretinopathy using perfluoro-n-octane: a multicenter study. Am J Ophthalmol 2003, 136:454–463
3. Fisher SK, Lewis GP, Linberg KA, Verardo MR: Cellular remodeling in mammalian retina: results from studies of experimental retinal detachment. Prog Retin Eye Res 2005, 24:395–431
4. Sethi CS, Lewis GP, Fisher SK, Leitner WP, Mann DL, Luthert PJ, Charteris DG: Glial remodeling and neural plasticity in human retinal detachment with proliferative vitreoretinopathy. Invest Ophthalmol Vis Sci 2005, 46:329–342
5. Lewis GP, Fisher SK: Muller cell outgrowth after retinal detachment: association with cone photoreceptors. Invest Ophthalmol Vis Sci 2000, 41:1542–1545
6. Guérin CJ, Anderson DH, Fisher SK: Changes in intermediate filament

immunolabeling occur in response to retinal detachment and reattachment in primates. Invest Ophthalmol Vis Sci 1990, 31:1474–1482
7. Cantó Soler MV, Gallo JE, Dodds RA, Suburo AM: A mouse model of proliferative vitreoretinopathy induced by dispase. Exp Eye Res 2002, 75:491–504
8. Fisher SK, Erickson PA, Lewis GP, Anderson DH: Intraretinal proliferation induced by retinal detachment. Invest Ophthalmol Vis Sci 1991, 32:1739–1748
9. Messmer EM, Heidenkummer HP, Kampik A: Ultrastructure of epiretinal membranes associated with macular holes. Graefes Arch Clin Exp Ophthalmol 1998, 236:248–254
10. Mietz H, Walshe R, Wiedemann P, Heimann K, Green WR: Histopathologic study of epiretinal proliferations after vitrectomy with daunomycin and silicone oil. Retina 1994, 14:425–429
11. Smiddy WE, Michels RG, Gilbert HD, Green WR: Clinicopathologic study of idiopathic macular pucker in children and young adults. Retina 1992, 12:232–236
12. Yamashita H, Hori S, Masuda K: Population and proportion of component cells in preretinal membranes. Jpn J Ophthalmol 1986, 30:269–281
13. Schwartz D, de la Cruz ZC, Green WR, Michels RG: Proliferative vitreoretinopathy. Ultrastructural study of 20 retroretinal membranes removed by vitreous surgery. Retina 1988, 8:275–281
14. Ripodas A, de Juan JA, Roldan-Pallares M, Bernal R, Moya J, Chao M, Lopez A, Fernandez-Cruz A, Fernandez-Durango R: Localisation of endothelin-1 mRNA expression and immunoreactivity in the retina and optic nerve from human and porcine eye. Evidence for endothelin-1 expression in astrocytes. Brain Res 2001, 912:137–143
15. Torbidoni V, Iribarne M, Ogawa L, Prasanna G, Suburo AM: Endothelin-1 and endothelin receptors in light-induced retinal degeneration. Exp Eye Res 2005, 81:265–275
16. Prasanna G, Hulet C, Desai D, Krishnamoorthy RR, Narayan S, Brun AM, Suburo AM, Yorio T: Effect of elevated intraocular pressure on endothelin-1 in a rat model of glaucoma. Pharmacol Res 2005, 51:41–50
17. Schinelli S: Pharmacology and physiopathology of the brain endothelin system: an overview. Curr Med Chem 2006, 13:627–638
18. Clozel M, Salloukh H: Role of endothelin in fibrosis and anti-fibrotic potential of bosentan. Ann Med 2005, 37:2–12
19. Roldán-Pallarés M, Rollin R, Mediero A, Martinez-Montero JC, Fernandez-Cruz A, Bravo-Llata C, Fernandez-Durango R: Immunoreactive ET-1 in the vitreous humor and epiretinal membranes of patients with proliferative vitreoretinopathy. Mol Vis 2005, 11:461–471
20. Davenport AP, Maguire JJ: Endothelin. Handb Exp Pharmacol 2006, 176(Pt1):295–329
21. Chakrabarti S, Gan XT, Merry A, Karmazyn M, Sima AA: Augmented retinal endothelin-1, endothelin-3, endothelinA and endothelinB gene expression in chronic diabetes. Curr Eye Res 1998, 17:301–307
22. Rattner A, Nathans J: The genomic response to retinal disease and injury: evidence for endothelin signaling from photoreceptors to glia. J Neurosci 2005, 25:4540–4549
23. D'Orléans-Juste P, Labonte J, Bkaily G, Choufani S, Plante M, Honore JC: Function of the endothelin(B) receptor in cardiovascular physiology and pathophysiology. Pharmacol Ther 2002, 95:221–238
24. Torbidoni V, Iribarne M, Suburo AM: Endothelin receptors in light-induced retinal degeneration. Exp Biol Med (Maywood) 2006, 231:1095–1100
25. Iandiev I, Uhlmann S, Pietsch UC, Biedermann B, Reichenbach A, Wiedemann P, Bringmann A: Endothelin receptors in the detached retina of the pig. Neurosci Lett 2005, 384:72–75
26. Iribarne M, Canto-Soler MV, Torbidoni V, Suburo AM: Controlling retinal pigment epithelium injury after experimental detachment of the retina. Invest Ophthalmol Vis Sci 2007, 48:1348–1354
27. Canto Soler MV, Gallo JE, Dodds RA, Hokfelt T, Villar MJ, Suburo AM: Y1 receptor of neuropeptide Y as a glial marker in proliferative vitreoretinopathy and diseased human retina. Glia 2002, 39:320–324
28. Barthel LK, Raymond PA: Improved method for obtaining 3-microns cryosections for immunocytochemistry. J Histochem Cytochem 1990, 38:1383–1388
29. Suburo AM, Chaud M, Franchi A, Polak JM, Gimeno MA: Distribution of neuronal and non-neuronal NADPH diaphorases and nitric oxide synthases in rat uterine horns under different hormonal conditions. Biol Reprod 1995, 52:631–637
30. Clozel M, Ramuz H, Clozel JP, Breu V, Hess P, Loffler BM, Coassolo P, Roux S: Pharmacology of tezosentan, new endothelin receptor antagonist designed for parenteral use. J Pharmacol Exp Ther 1999, 290:840–846
31. Jacques D, Sader S, Perreault C, Abdel-Samad D, Jules F, Provost C: NPY, ET-1, and Ang II nuclear receptors in human endocardial endothelial cells. Can J Physiol Pharmacol 2006, 84:299–307
32. Boivin B, Chevalier D, Villeneuve LR, Rousseau E, Allen BG: Functional endothelin receptors are present on nuclei in cardiac ventricular myocytes. J Biol Chem 2003, 278:29153–29163
33. Laqua H, Machemer R: Glial cell proliferation in retinal detachment (massive periretinal proliferation). Am J Ophthalmol 1975, 80:602–618
34. Schinelli S, Zanassi P, Paolillo M, Wang H, Feliciello A, Gallo V: Stimulation of endothelin B receptors in astrocytes induces cAMP response element-binding protein phosphorylation and c-fos expression via multiple mitogen-activated protein kinase signaling pathways. J Neurosci 2001, 21:8842–8853
35. Blomstrand F, Venance L, Siren AL, Ezan P, Hanse E, Glowinski J, Ehrenreich H, Giaume C: Endothelins regulate astrocyte gap junctions in rat hippocampal slices. Eur J Neurosci 2004, 19:1005–1015
36. Shi-Wen X, Rodriguez-Pascual F, Lamas S, Holmes A, Howat S, Pearson JD, Dashwood MR, du Bois RM, Denton CP, Black CM, Abraham DJ, Leask A: Constitutive ALK5-independent c-Jun N-terminal kinase activation contributes to endothelin-1 overexpression in pulmonary fibrosis: evidence of an autocrine endothelin loop operating through the endothelin A and B receptors. Mol Cell Biol 2006, 26:5518–5527
37. Ostrow LW, Langan TJ, Sachs F: Stretch-induced endothelin-1 production by astrocytes. J Cardiovasc Pharmacol 2000, 36:S274–S277
38. Ostrow LW, Sachs F: Mechanosensation and endothelin in astrocytes—hypothetical roles in CNS pathophysiology. Brain Res Brain Res Rev 2005, 48:488–508
39. Ehrenreich H, Anderson RW, Ogino Y, Rieckmann P, Costa T, Wood GP, Coligan JE, Kehrl JH, Fauci AS: Selective autoregulation of endothelins in primary astrocyte cultures: endothelin receptor-mediated potentiation of endothelin-1 secretion. New Biol 1991, 3:135–141
40. MacCumber MW, Ross CA, Snyder SH: Endothelin in brain: receptors, mitogenesis, and biosynthesis in glial cells. Proc Natl Acad Sci USA 1990, 87:2359–2363
41. Prasanna G, Krishnamoorthy R, Clark AF, Wordinger RJ, Yorio T: Human optic nerve head astrocytes as a target for endothelin-1. Invest Ophthalmol Vis Sci 2002, 43:2704–2713
42. Kasuya Y, Abe Y, Hama H, Sakurai T, Asada S, Masaki T, Goto K: Endothelin-1 activates mitogen-activated protein kinases through two independent signalling pathways in rat astrocytes. Biochem Biophys Res Commun 1994, 204:1325–1333
43. Nakazawa T, Takeda M, Lewis GP, Cho KS, Jiao J, Wilhelmsson U, Fisher SK, Pekny M, Chen DF, Miller JW: Attenuated glial reactions and photoreceptor degeneration after retinal detachment in mice deficient in glial fibrillary acidic protein and vimentin. Invest Ophthalmol Vis Sci 2007, 48:2760–2768
44. Wilhelmsson U, Li L, Pekna M, Berthold CH, Blom S, Eliasson C, Renner O, Bushong E, Ellisman M, Morgan TE, Pekny M: Absence of glial fibrillary acidic protein and vimentin prevents hypertrophy of astrocytic processes and improves post-traumatic regeneration. J Neurosci 2004, 24:5016–5021
45. Egnaczyk GF, Pomonis JD, Schmidt JA, Rogers SD, Peters C, Ghilardi JR, Mantyh PW, Maggio JE: Proteomic analysis of the reactive phenotype of astrocytes following endothelin-1 exposure. Proteomics 2003, 3:689–698
46. Rosanò L, Spinella F, Di Castro V, Nicotra MR, Dedhar S, de Herreros AG, Natali PG, Bagnato A: Endothelin-1 promotes epithelial-to-mesenchymal transition in human ovarian cancer cells. Cancer Res 2005, 65:11649–11657
47. Shi-Wen X, Denton CP, Dashwood MR, Holmes AM, Bou-Gharios G, Pearson JD, Black CM, Abraham DJ: Fibroblast matrix gene expression and connective tissue remodeling: role of endothelin-1. J Invest Dermatol 2001, 116:417–425
48. Shi-Wen X, Chen Y, Denton CP, Eastwood M, Renzoni EA, Bou-Gharios G, Pearson JD, Dashwood M, du Bois RM, Black CM, Leask A, Abraham DJ: Endothelin-1 promotes myofibroblast induction through the ETA receptor via a rac/phosphoinositide 3-kinase/Akt-dependent pathway and is essential for the enhanced contrac-

tile phenotype of fibrotic fibroblasts. Mol Biol Cell 2004, 15:2707–2719
49. Chi X, Anselmi K, Watkins S, Gandhi CR: Prevention of cultured rat stellate cell transformation and endothelin-B receptor upregulation by retinoic acid. Br J Pharmacol 2003, 139:765–774
50. Lecain E, Alliot F, Laine MC, Calas B, Pessac B: Alpha isoform of smooth muscle actin is expressed in astrocytes in vitro and in vivo. J Neurosci Res 1991, 28:601–606
51. Guidry C: Isolation and characterization of porcine Muller cells. Myofibroblastic dedifferentiation in culture. Invest Ophthalmol Vis Sci 1996, 37:740–752
52. Gamulescu MA, Chen Y, He S, Spee C, Jin M, Ryan SJ, Hinton DR: Transforming growth factor beta2-induced myofibroblastic differentiation of human retinal pigment epithelial cells: regulation by extracellular matrix proteins and hepatocyte growth factor. Exp Eye Res 2006, 83:212–222
53. Vyalov S, Desmouliere A, Gabbiani G: GM-CSF-induced granulation tissue formation: relationships between macrophage and myofibroblast accumulation. Virchows Arch B Cell Pathol Incl Mol Pathol 1993, 63:231–239
54. Narayan S, Brun AM, Yorio T: Endothelin-1 distribution and basolateral secretion in the retinal pigment epithelium. Exp Eye Res 2004, 79:11–19
55. Rowen SL, Glaser BM: Retinal pigment epithelial cells release a chemoattractant for astrocytes. Arch Ophthalmol 1985, 103:704–707
56. Bryan III JA, Campochiaro PA: A retinal pigment epithelial cell-derived growth factor(s). Arch Ophthalmol 1986, 104:422–425